QI Wei (Orcid ID: 0000-0001-6969-6729)
Feng Lian (Orcid ID: 0000-0002-4590-3022)
Liu Junguo (Orcid ID: 0000-0002-5745-6311)

Snow as an important natural reservoir for runoff and soil moisture in Northeast China

Wei Qi [1, 2, 3], Lian Feng [1, 2, 3*], Junguo Liu [1, 2, 3], Hong Yang [4, 5]

[1] School of Environmental Science and Engineering, Southern University of Science and Technology, Shenzhen 518055, China

[2] Guangdong Provincial Key Laboratory of Soil and Groundwater Pollution Control

[3] State Environmental Protection Key Laboratory of Integrated Surface Water-Groundwater Pollution Control

[4] Eawag, Swiss Federal Institute of Aquatic Science and Technology, Duebendorf, Switzerland

[5] Department of Environmental Science, MGU, University of Basel, Basel, Switzerland

[*] Email: fengl@sustech.edu.cn

Abstract:

As one of the major agricultural regions in the world, water scarcity problems in Northeast China have drawn much attention recently. Because of cold and long winter period, snow is an important component in the hydrological system. Yet, few studies have been conducted to systematically assess its role. This study quantified the effects of snow on runoff and soil moisture in the entire region in a 30-year time period (1982-2011) for the first time. A water and energy budget-based distributed biosphere hydrological model with improved snow physics after calibration and validation is employed. A Standardized Snow depth Index (SSdI) is also proposed to quantify snow variations. Result show that snow contributes 11% to runoff annually on average and 66% and 33% in April and May (main months for crop planting). Soil moisture could decrease by at least 20% in March, April and May if there would be no snow, and the major agriculture area suffers more than other regions. We also found that SSdI is indicative of standardized soil moisture index and standardized runoff index in spring, particularly useful for supporting water management in agriculture. These results indicate that snow performs like an important reservoir: redistribute water resources among months. This study provides unique insights into the importance of snow in the entire region. The results improve the awareness of the importance of snow to water resources management, and indicate that it is worth paying attention to snow in water resources management in this region.

Keywords: Snow, Northeast China, Songhua River, Liao River, Reservoir, Water Resources

Plain language summary

Because of cold and long winter period in Northeast China, snow plays a role as natural reservoir to store water in winter and to release water to ameliorate water shortage in spring. In addition, snow can influence agriculture through affecting soil moisture. However, studies on the role of snow in the region are limited so far. Here, we evaluate the importance of snow as a reservoir in entire Northeast China for the first time. We found on average snow contributes 11% to the annual runoff, and 66% and 33% in April and May (the main crop planting months). Soil moisture in the region can decrease by at least 20% in March, April and May if there would be no snow, and the major agriculture area suffers more than other regions. Therefore, snow is an important source of water resources in this region, and worth paying attention to in water resources management.

Highlights:

We quantified snow contribution to runoff in entire Northeast China for the first time, and found it is 11% on average and 66% in April

Snow plays an important role in keeping soil moisture. In March, April and May, soil moisture decreases by at least 20% when no snow

SSdI is proposed to quantify snow variations, and it is indicative of runoff and soil moisture variations in spring

1. Introduction

Northeast China covers a total area of around 1.22 million square kilometres, and is an important region for agricultural production, such as soybean, maize and rice. Due to increasing population and intensification of agricultural production, the water shortage problems in the region have drawn much attention recently.

Because of cold and long winter period in Northeast China, snow plays a role as natural reservoir to store water in winter and to release water to ameliorate water shortage in spring. In addition, snow also can influence agriculture through affecting soil moisture [Long et al., 2019]. It is, hence, necessary to understand the role of snow in Northeast China for supporting the water resources management in this region. However, studies on the role of snow in the region are limited so far. Zhang et al. [2010] used the Moderate-resolution Imaging Spectro-radiometer (MODIS) snow cover product to investigate snow cover variations in Liaoning Province which is located in southern part of Northeast China and covers an area of only about 12% of the total area of Northeast China. Ding and Gao [2015] studied the number of snow days in Northeast China based on meteorological station data. Feng and Chen [2016] investigated snow intensity changes in Northeast China based on meteorological station data. Tian et al. [2018] studied snow changes in the upper Second Songhua River basin in Northeast China, which has an area of only about 1.5% of the total area of Northeast China. Despite the progresses, the previous studies did not analyse snow influence on runoff/soil moisture specifically, or investigated regions that only cover a small fraction of Northeast China. A systematic study on snow contribution to runoff and influence on soil moisture covering the entire region is not available.

In snow covered regions, snow plays an important role in spring to ameliorate water shortage [Li et al., 2017; Dierauer et al., 2019; Milly et al., 2020]. Staudinger et al. [2014] introduced a standardized melt and rainfall index to consider snow influence on runoff. This standardized melt and rainfall index was based on the sum of precipitation and snowmelt water, and therefore can consider snow influence. However, it is not indicative of soil moisture deficit. Zhang et al. [2019] developed a standardized moisture anomaly index which incorporates snowmelt runoff in soil moisture anomaly analysis. Despite the progress in considering snow, the previous studies are generally based on snowmelt water. It represents the situation that water has been released from storage, and is not indicative of how much water is stored as a solid form at present for future use. Therefore, the snowmelt-based index is weak in predicting snow induced water shortage. Thus, it is useful to develop a snow related index that is indicative of snow related water resources changes in the coming months of a year.

The overall objective of this study is to evaluate the contribution of snow to runoff/discharge and influence of snow on soil moisture in Northeast China. A Standardized Snow depth Index (SSdI) is proposed to quantify snow depth variations, which represents water stored at present for future potential use. The larger the snow storage, the greater the capacity of the natural reservoir to ameliorate later water shortage. This paper is unique in that, for the first time ever, it evaluates the importance of snow as a reservoir in entire Northeast China.

2. Study region and datasets

2.1 Northeast China

Fig. 1 shows the location of Northeast China. Its western and northwestern parts are the Greater Khingan Range, and its eastern and southeastern parts are the Lesser Khingan Mountains and Changbai Mountain. The southern parts are the Yanshan Mountain, Bohai Sea and Huanghai

Sea. There are two large rivers in Northeast China: Liao River and Songhua River. Liao River is located in the southern parts of Northeast China; Songhua River is located in the northern and eastern parts, and is the largest tributary of the Heilongjiang River (the Amur River). The Heilongjiang River forms the national boundary between Russia and China. The Songliao Plain is located in central parts of Northeast China, and the Sanjiang Plain is located in the eastern parts. The Songliao Plain and Sanjiang Plain form the largest plain in China, i.e., Northeast China Plain. It is one of the largest chernozem regions in the world, and is also one of the major regions for soybean and maize production [Yang et al., 2007; Kent et al., 2017]. Because Northeast China is a heavily managed region for agriculture and industry, the water resources utilization rate is higher than 40% according to the report of the Songliao Water Conservancy Committee of the Ministry of Water Resources of China (http://www.slwr.gov.cn/szy2011/). There are many reservoirs along the main rivers for hydropower generation and irrigation, as well as urban uses.

2.2 Datasets

The Asian Precipitation - Highly-Resolved Observational Data Integration Towards Evaluation of Water Resources (APHRODITE) [Xie et al., 2007; Yatagai et al., 2012] data is used. APHRODITE is purely based on precipitation gauge data, and it used data from both Northeast China and the Russian Far East. APHRODITE is considered the best precipitation data and has been used in many studies (e.g., Qi et al. [2016a]; Chen et al. [2018]; Pritchard [2019]). Downward shortwave and longwave radiation, specific humidity, wind speed and air temperature are from the China Meteorological Forcing Dataset (CMFD) developed by the Institute of Tibetan Plateau Research, Chinese Academy of Sciences [He et al., 2020]. APHRODITE and CMFD data from 1982 to 2011 (30 years) are used in the study. CMFD has a spatial resolution of 0.1 degree, and APHRODITE has a spatial resolution of 0.25 degree.

Soil hydraulic property data are from the Future Water's Global Maps of Soil Hydraulic Property product (http://www.futurewater.eu/). The vegetation Leaf Area Index (LAI) and Fraction vegetation absorbed Photosynthetically Active Radiation (FPAR) were utilized to represent vegetation dynamic. The LAI and FPAR data are available from July 1981 to December 2011 developed by Zhu et al. [2013], and have a monthly temporal resolution and a 1/12 degree spatial resolution. Land-use data were collected from the United States Geological Survey (http://edc2.usgs.gov/glcc/glcc.php). Digital elevation model (30-meter resolution) is collected from the NASA Shuttle Radar Topographic Mission [Rabus et al., 2003]. The remote sensing based snow depth data were collected from Dai Liyun and Che Tao [2015] (http://www.tpdc.ac.cn/zh-hans/data/df40346a-0202-4ed2-bb07-b65dfcda9368/). It was developed specifically for China on the basis of different microwave remote sensing datasets [Che et al., 2008; Dai et al., 2012; Dai et al., 2015]. The global monthly MOD10CM data from MODIS are available after March 2000, and have a spatial resolution of 0.05 degree. MOD10CM data from 2001 to 2011 are used to evaluate modeled snow cover fraction. The spatially distributed rain-snow temperature threshold dataset developed by Jennings et al. [2018] is used in the model. The Global Land Evaporation Amsterdam Model (GLEAM) dataset is based on reanalysis and remote sensing based soil moisture data, and available after 1980. GLEAM has a spatial resolution of 0.25 degree and has been used in many studies [Jung et al., 2010; Miralles et al., 2011; Martens et al., 2016; Martens et al., 2017; Li et al., 2019]. Therefore, GLEAM is used in his study to evaluate model performance in soil moisture simulation. All the data are regridded into 0.1 degree cells in this study.

3. Methodology

3.1 WEB-DHM-S model, calibration and validation

The Water and Energy Budget-based Distributed biosphere Hydrological Model with improved Snow physics (WEB-DHM-S) is used in this study. It combined the Simple Biosphere scheme (SiB2) land surface model, the hydrological model based on geomorphology developed by Yang [1998], and a physically based snowmelt module [Wang et al., 2009a; Wang et al., 2009b; Wang et al., 2009c; Shrestha et al., 2010; Wang et al., 2017]. The snowmelt is calculated based on water and energy balances in snow layers. The snowmelt module uses a three-layer snowmelt simulation approach from the Simplified Simple Biosphere 3 (SSiB3) and the Biosphere-Atmosphere Transfer Scheme (BATS) albedo scheme [Shrestha et al., 2010; Shrestha et al., 2015; Qi et al., 2019a]. This model has been used in many studies, and shows good performance generally [Shrestha et al., 2010; Qi et al., 2015; Qi et al., 2016a; Wang et al., 2017; Qi et al., 2018; Qi et al., 2019b]. WEB-DHM-S input data includes precipitation, air temperature, downward solar and longwave radiation, air pressure, wind speed and humidity (see Section 2.2).

We used 16 river basins off the main rivers and cropland to calibrate WEB-DHM-S. These river basins are located in the upper streams or in water resources conservation areas (Fig. 1), therefore are less influenced by human activities than the regions close to the main rivers and cropland. The Dynamically Dimensioned Search algorithm was used in the calibration because of its high efficiency [Tolson and Shoemaker, 2008; Tolson et al., 2009; Qi et al., 2016b]. The calibration was carried out on a monthly scale due to the unavailability of daily scale observed runoff data. There are 16 years of data in the Suolun hydrological gauge (1982-1997), and 20 years of data in the Yichun and Chenming hydrological gauges (1982-2001). To ensure there are several years of discharge data for model validation in each hydrological gauge, the

discharge data from 1982 to 1990 were used to calibrate WEB-DHM-S parameters, and the discharge data after 1991 are kept for model validation. Time periods of available discharge data for calibration and validation are shown in Table S1.

Nash-Sutcliffe Efficiency (NSE) and Relative Bias (RB) are the most commonly used criteria for discharge simulation evaluations, and they are equally important for such purpose (e.g., Wang et al. [2016], Qi et al. [2019a]). The evaluation standard for hydrological information and hydrological forecasting in China also recommends using NSE and RB as criteria [People's Republic of China, 2008]. The value of NSE ranges between $-\infty$ and 1, and |RB| ranges between 0 and ∞. As both criteria are important, we used a combination of them in the objective function for model parameter calibration. In this study, the objective function is set as:

$$\text{minimize}\left[mean\left(\left|NSE-1\right|\right) + mean\left(\left|RB\right|\right)\right] \quad (1)$$

where 'mean' represents the average in the 16 river basins. The range of |NSE-1| is from 0 to ∞, matching the range of |RB|. Both |NSE-1| and |RB| reach their best values when they are zeros, therefore their magnitudes are comparable in terms of their best values. |NSE-1| and |RB| are used in the objection function with equal weights. The minimum value of the objective function is sought in evaluating the simulation performance. The advantage of using this objective function is that the model performance evaluation simultaneously considered the two criteria. Similar objective function has been successfully used in hydrological model calibration in previous studies (e.g., Qi et al. [2018], Qi et al. [2020]). The lower the objective function values, the better the parameter values. The calibration repeated 1000 times, and the parameter sets with the lowest objective function values are selected.

3.2 Standardized Snow depth Index (SSdI)

Analogous to non-parametric standardized precipitation index [Hao et al., 2014; Farahmand and AghaKouchak, 2015], the non-parametric Standardized Snow depth Index (SSdI) is based on standardized snow depth data to quantify snow variations. There are two steps to calculate SSdI. First, empirical probability of snow depth is calculated based on empirical Gringorten plotting position as follows

$$p(x_i) = \frac{i - 0.44}{n + 0.12} \tag{2}$$

where n is the sample size; i is the rank of snow depth data from the smallest; x represents snow depth; p represents corresponding empirical probability. Second, the SSdI is calculated using the following equation

$$\mathrm{SSdI} = f^{-1}(p) \tag{3}$$

where f represents the standard normal distribution function. The snow shortage comparison in different magnitude is facilitated by using the normal distribution transformation. The correlation between SSdI and Standardized Soil moisture Index (SSI)/Standardized Runoff Index (SRI) is calculated based on the following equation

$$R = corr\left(SSdI_{i,n-m}, S_{i+m,n}\right) \tag{4}$$

where *corr* represents the function of correlation coefficient, S represents SSI and SRI; m represents time lag between calculated SSdI and SSI/SRI time series; i represents accumulation time of calculated SSdI, SSI and SRI. SSI and SRI are based on the study by Hao et al. [2014] and Farahmand and AghaKouchak [2015]. SSI and SRI represent soil moisture and runoff variations. The correlation analysis can evaluate the influence of accumulated snowpack (i.e. snow depth) on later soil moisture and runoff.

Our study is based on the data stretching over a range of 30 years. This time span is common in climatology studies. For example, Donat et al. [2016] studied precipitation changes using 30-year moving time window; Padrón et al. [2020] and Konapala et al. [2020] used 30-year time periods to investigate water availability changes; Livneh et al. [2020] used 30-year time periods to study snow variations under climate change. Building on these studies, we believe that the 30-year time period covered in our study is sufficient for simulating snow contributions to runoff.

3.3 Criteria for assessment

NSE and RB used in discharge simulation evaluation are as below:

$$\mathrm{NSE} = 1 - \frac{\sum_{i=1}^{n}\left(Q_{pi} - Q_{ti}\right)^2}{\sum_{i=1}^{n}\left(Q_{ti} - \overline{Q_t}\right)^2} \tag{5}$$

$$\mathrm{RB} = \frac{\sum_{i=1}^{n} Q_{pi} - \sum_{i=1}^{n} Q_{ti}}{\sum_{i=1}^{n} Q_{ti}} \times 100\% \tag{6}$$

where Q_{pi} and Q_{ti} represent simulated and observed discharge at time i; $\overline{Q_t}$ represents average of observed discharge.

Correlation Coefficient (R), Root Mean Square Error (RMSE), NSE and RB are commonly used in snow related evaluations [Chen et al., 2017; Henn et al., 2018; Han et al., 2019; Koch et al., 2019], and therefore they are used in the snow simulation evaluations in this study:

$$\mathrm{RMSE} = \sqrt{\frac{\sum_{i=1}^{n}\left(X_{si} - X_{oi}\right)^2}{n}} \tag{7}$$

where X_{si} and X_{oi} represent simulation data and observation at time i; n represents the number of data points.

4. Result and discussion

4.1 Model evaluation

The calibrated model parameters are shown in Table S2. The average model performances in discharge simulation are shown Table S3, and performance for every selected sub-basins are shown in Table S4. The performances are acceptable in both calibration and validation periods, with |RB| being 8.0% and 11.0% respectively (Table S2). The overall |RB| value is 7.8%, and NSE value is 0.81. The overall NSE values are over 0.9 in some sub-basins, such Shalizhai, Lishugou and Wendegen (Table S4). The overall NSE value is 0.64 in Suolun gauge, which may be because the available data is from 1982 to 1997 and is less than other gauges. The comparisons between observed discharge and simulation are shown in Fig. 2. Observed and simulated hydrographs in the calibration and validation periods are shown in Fig. S1 and Fig. S2. In sum, the overall model performance is satisfactory in discharge simulation. These results indicate that the objective function (i.e. Eq. (1)) used in the model parameter calibration is appropriate.

Figs. 3(a) and (b) show average snow depth and snow cover fraction comparison between model simulation and remote sensing data on a multi-year mean monthly scale. The model simulation and remote sensing data agree well. NSE, RB, R and RMSE are 0.69, 2.0%, 0.85 and 2.28 in terms of snow depth, and are 0.85, -1.0%, 0.96 and 0.13 in terms of snow cover fraction. Figs. 3(c) and (d) show the comparison of surface zone soil moisture between the WEB-DHM-S model simulation and the GLEAM dataset. The model simulates the seasonal variations of soil moisture well. The R values are up to 0.87 and 0.86 for average surface zone soil moisture in Northeast China and on the cropland in the region, respectively. The model also simulates cropland surface soil moisture well. The average surface soil moisture in cropland is 0.39 m^3/m^3 and 0.34 m^3/m^3 for the model simulation and GLEAM, respectively. In

April and May, the average surface soil moisture in cropland is 0.35 m^3/m^3 and 0.31 m^3/m^3 for model simulation and GLEAM, respectively. The model simulates the surface zone soil moisture at 5 cm depth, and the surface zone soil moisture from GLEAM is at 10 cm depth. The differences in the soil depth may contribute the differences in the soil moisture content. Overall, the model can simulate the soil moisture well.

In this study, the saturated water content dataset is from the Future Water's Global Maps of Soil Hydraulic Property product (http://www.futurewater.eu/). This product shows the saturated water content ranges from 0.3 to 0.9. The uncertainty of the saturated water content parameter value used in this study may result from this product. However, the model parameter value used is between the minimum and maximum values, and therefore the parameter value used in this study is appropriate. Chen et al. [2017] developed a two-stage approach to calibrate a hydrological model against snow cover fraction, snow water equivalent, total water storage and streamflow in the Upper Brahmaputra River basin in the Tibetan Plateau. Similarly, several recent studies are also suggested using multiple datasets in model calibration and validation [Henn et al., 2018; Ko et al., 2019; Dembélé et al., 2020; Long et al., 2020]. In our study, we used streamflow in the model calibration combined with an observation based rain-snow temperature threshold data product. Validations using observed streamflow, snow depth, snow cover fraction and satellite based soil moisture show that the performance of the model is satisfactory. This result implies that the model used and the combination of the model and the observation datasets for discharge, soil moisture and snow simulations are appropriate. In addition, this result also indicates that the model used is robust: one constraint leads to satisfactory simulation results for several variables, which, to some degree, may be because streamflow is one of the most sensitive variables to uncertainty in a model simulation chain [Qi et al., 2020].

4.2 Importance of snow to runoff and discharge

Fig. 4 shows the spatial distribution of river discharge. The average discharge in Jul-Aug-Sep is larger than averages in other periods, and the river discharge in the Songhuajiang River is generally larger than that in the Liao River. Fig. 5 shows the spatial distribution of snow discharge. The average snow discharges in Apr-May-Jun and Oct-Nov-Dec are higher than other periods. In the summer period (Jul-Aug-Sep), most of the precipitation is from rainfall due to high air temperature, and therefore snow discharge during this period is lower than other periods.

Figs. 6(a) and (b) show the temporal changes of snowmelt runoff and its contribution to total runoff. Snowmelt runoff is higher in April and October than other months, i.e., two snowmelt runoff peaks, which is similar to a study in the Upper Yangtze River in the Tibetan Plateau [Han et al., 2019]. The snowmelt runoff contribution to total runoff is higher in April and November. Although the snowmelt runoff is higher in October than November, the total runoff in November is much smaller than October, which may lead to the higher snowmelt runoff contribution than October. On average, snowmelt runoff contributes 11.3% to the annual total runoff, which is about 21.8 billion m^3 water resources. This volume of water is equivalent to about 55.5% of the total storage capacity of the Three Gorges reservoir, the largest reservoir in the world. In April and May (the major crop planting months), snowmelt runoff contributes at least 33.1% to the runoff. In April, the contribution reaches the highest values up to 65.5%.

Figs. 6(c), (d), (e) and (f) show the spatial distribution of snowmelt discharge contributions to total river discharge. The snow discharge contribution changes dramatically in both temporal and spatial scales. The average in Jan-Feb-Mar is generally high (25.2%) with the exception in some regions in southwest part, which may be because the region is very dry with very low

snow/precipitation in Jan-Feb-Mar. Compared to other time periods, the average snow discharge contribution in Jul-Aug-Sep is lower (0.8%), which may be due to the existence of precipitation as rainfall in this period.

Fig. 7 shows mean precipitation, mean snowfall, mean air temperature, minimum and maximum air temperature in different months in Northeast China. It can be seen that there are two snowfall peaks (April and October). They are resulted from the combined effects of precipitation and air temperature. In April and October, there are plenty of precipitation when temperature is not high, whereas either air temperature is very high or precipitation is low in other months resulting in less snowfall than April and October. The two snowmelt runoff peaks in April and October are because of the two snowfall peaks and relatively high air temperate in these two months. In December, January and February, it can be seen that the maximum air temperature are about/above zero degree although the mean air temperature is much lower than zero degree, which results in snowmelt in some regions in Northeast China. In addition, the total runoff is little in December, January and February because of little precipitation. The combined effects of precipitation, snowfall and air temperature in December, January and February result in the relatively large snowmelt runoff contribution to the total runoff.

4.3 Importance of snow to soil moisture

To evaluate the importance of snow to soil moisture, we compared the soil moisture of 'No snow scenario' and 'Normal simulation'. Here, the 'No snow scenario' assumes that the snowfall is replaced by rainfall. Figs. 8(a), (b), (c) and (d) show the spatial distribution of surface soil moisture and changes when snow exists, i.e., under the 'Normal simulation'. The 'Change' is calculated as soil moisture$_{\text{No snow scenario}}$ minus soil moisture$_{\text{Normal simulation}}$. It can be seen that the Songliao Plain has lower soil moisture than the surrounding high mountain areas.

This is likely because the high mountain areas are covered by trees and/or dense shrubs, which can prevent evaporation of surface soil moisture. In the 'No snow scenario', the surface soil gets dryer generally, especially in the plain regions, which is also shown in the 'Change'. Therefore, the plain regions (the main cropland areas) suffer more than other regions when snow does not exist.

Figs. 8(e) and (f) show the average surface zone soil moisture changes in Northeast China and on the cropland area. The surface zone soil gets dryer generally when no snow exists. In March, April and May, the soil moisture decreases by 20.1%, 23.5% and 22.4%, which equal to -0.08 m^3/m^3, -0.09 m^3/m^3 and -0.07 m^3/m^3, respectively. Because soil moisture is an important source of water for agriculture, the decreases may lead to drought and increase in irrigation requirement. This result suggests that snow can ameliorate water shortage problems in the region.

4.4 Standardized Snow depth Index (SSdI)

There are time lags between snow depth and soil water and/or streamflow volumes. Table 1 shows the correlation coefficient between SSdI, SRI and SSI. The correlation coefficient is calculated based on Eq. (3). Comparison among SRI, SSI and SSdI under different accumulation time are shown in Fig. S4. Results from 1-month to 7-month are shown in Table 1. The correlation coefficient values become very small under the 7-month situation, and therefore we did not investigate the situations after 7-month. The correlation is evaluated at a 0.05 a significance level.

It is noticed that R is decreasing with increasing time lags, and 1 month time lag has the largest R values generally. For example, for the 1-month accumulation time, R between SSdI and SSI

decreases from 0.35 to 0.12 before the correlation becomes non-significant, and R between SSdI and SRI decreases from 0.30 to 0.14. In addition, it can be seen that R between SSdI and SSI is the highest (0.37) when accumulation time is 2-month and time lag is 1 month. This indicates that snow in January and February has large influence on soil moisture in February and March. For SRI, the R value is the highest (0.39) when accumulation time are 2-month and 3-month and time lag is 1 month. It indicates that snow in January and February has large influence on runoff in February and March, and that snow in January, February and March has large influence on runoff in February, March and April. The 4-month SSdI and SRI have an R of 0.37, higher than other accumulation time situations except for the 2-month and 3-month cases, which indicates that snow in January, February, March and April have large influence on runoff in February, March, April and May. In the 4-month accumulation time, 1-3 month lags have significant correlation, and the correlation becomes non-significant for SRI when time lag is 4-month. Overall, the results indicate that one month lag has the largest influence, the influence is decreasing with increasing time lag, and the correlation is significant with a time lag of 1-3 months.

The snow related indexes developed by Staudinger et al. [2014] and Zhang et al. [2019] are based on snowmelt water, and therefore are not indicative of snow stored water in solid form for future potential use. Compared to the previous indexes, SSdI represents snow depth variations indicating stored solid water resources which could melt in coming months for use. Dai et al. [2004] and Dai [2011] suggested that the Palmer Drought Severity Index (PDSI) and soil moisture in the coming months have significant correlations, and therefore PDSI is considered as a proxy to predict soil moisture induced drought in the coming months. Similarly, the significant correlation between SSdI and SSI/SRI with a time lag of 1-3 months also gives SSdI an ability to predict the soil moisture and stream discharge condition in spring. Hence,

SSdI can be highly important to support agriculture production and water management, particularly during the planting season. Although PDSI can be used to predict soil moisture deficit, it did not consider snow influence. Compared to PDSI, SSdI can consider snow influence, and therefore is superior to PDSI in snow covered regions. It is recorded that from December 2019 to early April 2020, Northeast China had received little snow. SSdI during this period suggested drought during the spring. Fortunately, in late April 2020, there have been several major snow events covering most areas of Northeast China. SSdI is able to quantify the effects of these snow events to ameliorate the drought situation in May in the region.

5. Conclusions

As an important area for agricultural production in China, including soybean, maize and rice, and the largest chernozem region in the world, water resource problems in Northeast China have drawn much attention. Because of cold and long winter period, snow plays an important role in water resources in this region. However, studies on snow in Northeast China are quite few, and investigations into snow in entire Northeast China are rare. This study addressed the importance of snow by evaluating the contribution of snowmelt to discharge/runoff and influence of snow on soil moisture in a 30-year time period (1982-2011) in the whole of Northeast China for the first time. The SSdI method is proposed to quantify snow depth variations. A water and energy budget-based distributed biosphere hydrological model with improved snow physics after calibration and validation is employed. The following conclusions are presented on the basis of this study.

First, snow contributes a large proportion to runoff in the entire Northeast China region. On average, it contributes 11.3% to the total runoff on an annual basis. In April and May, snowmelt runoff contributes 65.5% and 33.1% to the runoff during the period.

Second, snow plays an important role in keeping soil moisture. In March, April and May, the soil moisture would decrease at least 20.1% when there is no snow. The Northeast China Plain (the main cropland area) suffers more than surrounding areas when snow does not exist.

Third, SSdI developed in this study is indicative of SSI and SRI in spring. The correlation between SSdI and SSI/SRI is decreasing with increasing time lag, and it is significant with a time lag of 1-3 months. The time lag between SSdI and SSI/SRI enables a use of SSdI to predict the soil moisture and runoff conditions in spring, the planting season of Northeast China.

Acknowledgements:

This study was supported by the Young Scientists Fund of the National Natural Science Foundation of China (51809136). Additional support was provided by the Strategic Priority Research Program of the Chinese Academy of Sciences (Grant no. XDA20060402), the High-level Special Funding of the Southern University of Science and Technology (Grant No. G02296302, G02296402). The forcing dataset used in this study (i.e., CMFD) was developed by the Data Assimilation and Modeling Center for Tibetan Multi-spheres, the Institute of Tibetan Plateau Research, Chinese Academy of Sciences (http://westdc.westgis.ac.cn/data/7a35329c-c53f-4267-aa07-e0037d913a21). The discharge data in Northeast China are from hydrology bureaus, and can be found by contacting Songliao Water Resources Commission (http://www.slwr.gov.cn/slwjj/slwgk/).

References:

Che, T., Li, X., Jin, R., Armstrong, R., Zhang, T., (2008). Snow depth derived from passive microwave remote-sensing data in China. *Annals of Glaciology*, 49(1): 145-154. DOI:10.3189/172756408787814690

Chen, A., Chen, D., Azorin‐Molina, C., (2018). Assessing reliability of precipitation data over the Mekong River Basin: A comparison of ground‐based, satellite, and reanalysis datasets. *International Journal of Climatology*, 38(11): 4314-4334. DOI:10.1002/joc.5670

Chen, X., Long, D., Hong, Y., Zeng, C., Yan, D., (2017). Improved modeling of snow and glacier melting by a progressive two‐stage calibration strategy with GRACE and multisource data: How snow and glacier meltwater contributes to the runoff of the Upper Brahmaputra River basin? *Water Resources Research*, 53(3): 2431-2466. DOI:10.1002/2016WR019656

Dai, A., Trenberth, K.E., Qian, T., (2004). A Global Dataset of Palmer Drought Severity Index for 1870–2002: Relationship with Soil Moisture and Effects of Surface Warming. *Journal of Hydrometeorology*: 1117-1130. DOI:10.1175/JHM-386.1

Dai, A., (2011). Drought under global warming: a review. *Wiley Interdisciplinary Reviews: Climate Change*: 45-65. DOI:10.1002/wcc.81

Dai, L., Che, T., Wang, J., Zhang, P., (2012). Snow depth and snow water equivalent estimation from AMSR-E data based on a priori snow characteristics in Xinjiang, China. *Remote Sensing of Environment*, 127: 14-29. DOI:10.1016/j.rse.2011.08.029

Dai, L., Che, T., Sensing, D.Y., (2015). Inter-calibrating SMMR, SSM/I and SSMI/S data to improve the consistency of snow-depth products in China. *Inter-calibrating SMMR, SSM/I and SSMI/S data to improve the consistency of snow-depth products in China*.

Dai Liyun, Che Tao, (2015). Long-term sequence dataset of China snow depth (1979-2018). *National Tibetan Plateau Data Center*. DOI:10.11888/Geogra.tpdc.270194

Dembélé, M., Hrachowitz, M., Savenije, H.H.G., Mariéthoz, G., Schaefli, B., (2020). Improving the Predictive Skill of a Distributed Hydrological Model by Calibration on Spatial Patterns With Multiple Satellite Data Sets. *Water Resources Research*. DOI:10.1029/2019WR026085

Dierauer, J.R., Allen, D.M., Whitfield, P.H., (2019). Snow Drought Risk and Susceptibility in the Western United States and Southwestern Canada. *Water Resources Research*, 55(4): 3076-3091. DOI:10.1029/2018WR023229

Ding, T., Gao, H., (2015). Relationship between winter snow cover days in Northeast China and rainfall near the Yangtze River basin in the following summer. *Journal of Meteorological Research*, 29(3): 400-411. DOI:10.1007/s13351-014-4255-4

Donat, M.G., Lowry, A.L., Alexander, L.V., O'Gorman, P.A., Maher, N., Donat, M.G., Lowry, A.L., Alexander, L.V., O'Gorman, P.A., Maher, N., (2016). More extreme precipitation in the world's dry and wet regions. *Nature Climate Change*. DOI:10.1038/nclimate2941

Farahmand, A., AghaKouchak, A., (2015). A generalized framework for deriving nonparametric standardized drought indicators. *Advances in Water Resources*, 76: 140-145. DOI:10.1016/j.advwatres.2014.11.012

Feng, Y., Chen, H.-P., (2016). Warming over the North Pacific can intensify snow events in Northeast China. *Atmospheric and Oceanic Science Letters*, 9(2): 122-128. DOI:10.1080/16742834.2016.1133072

Han, P., Long, D., Han, Z., Du, M., Dai, L., Hao, X., (2019). Improved understanding of snowmelt runoff from the headwaters of China's Yangtze River using remotely sensed snow products and hydrological modeling. *Remote Sensing of Environment*, 224: 44-59. DOI:10.1016/j.rse.2019.01.041

Hao, Z., AghaKouchak, A., Nakhjiri, N., Farahmand, A., (2014). Global integrated drought monitoring and prediction system. *Scientific Data*, 1(1): 140001. DOI:10.1038/sdata.2014.1

He, J., Yang, K., Tang, W., Lu, H., Qin, J., Chen, Y., Li, X., He, J., Yang, K., Tang, W., Lu, H., Qin, J., Chen, Y., Li, X., (2020). The first high-resolution meteorological forcing dataset for land process studies over China. *Scientific Data*. DOI:10.1038/s41597-020-0369-y

Henn, B., Painter, T.H., Bormann, K.J., McGurk, B., Flint, A.L., Flint, L.E., White, V., Lundquist, J.D., Henn, B., Painter, T.H., Bormann, K.J., McGurk, B., Flint, A.L., Flint, L.E., White, V., Lundquist, J.D., (2018). High ‐ Elevation Evapotranspiration Estimates During Drought: Using Streamflow and NASA Airborne Snow Observatory

SWE Observations to Close the Upper Tuolumne River Basin Water Balance. *Water Resources Research*. DOI:10.1002/2017WR020473

Jennings, K.S., Winchell, T.S., Livneh, B., Molotch, N.P., (2018). Spatial variation of the rain–snow temperature threshold across the Northern Hemisphere. *Nature Communications*, 9(1): 1148. DOI:10.1038/s41467-018-03629-7

Jung, M., Reichstein, M., Ciais, P., Seneviratne, S.I., Sheffield, J., Goulden, M.L., Bonan, G., Cescatti, A., Chen, J., Jeu, R., (2010). Recent decline in the global land evapotranspiration trend due to limited moisture supply. *Nature*, 467(7318): 951.

Kent, C., Pope, E., Thompson, V., Lewis, K., Scaife, A.A., Dunstone, N., (2017). Using climate model simulations to assess the current climate risk to maize production. *Environmental Research Letters*, 12(5): 54012. DOI:10.1088/1748-9326/aa6cb9

Ko, A., Mascaro, G., Vivoni, E.R., (2019). Strategies to Improve and Evaluate Physics‐Based Hyperresolution Hydrologic Simulations at Regional Basin Scales. *Water Resources Research*: 1129-1152. DOI:10.1029/2018WR023521

Koch, F., Henkel, P., Appel, F., Schmid, L., Bach, H., Lamm, M., Prasch, M., Schweizer, J., Mauser, W., (2019). Retrieval of Snow Water Equivalent, Liquid Water Content, and Snow Height of Dry and Wet Snow by Combining GPS Signal Attenuation and Time Delay. *Water Resources Research*: 4465-4487. DOI:10.1029/2018WR024431

Konapala, G., Mishra, A.K., Wada, Y., Mann, M.E., (2020). Climate change will affect global water availability through compounding changes in seasonal precipitation and evaporation. *Nature Communications*: 3044. DOI:10.1038/s41467-020-16757-w

Li, D., Wrzesien, M.L., Durand, M., Adam, J., Lettenmaier, D.P., (2017). How much runoff originates as snow in the western United States, and how will that change in the future? *Geophysical Research Letters*, 44(12): 6163-6172. DOI:10.1002/2017GL073551

Li, X., Long, D., Han, Z., Scanlon, B.R., Sun, Z., Han, P., Hou, A., (2019). Evapotranspiration Estimation for Tibetan Plateau Headwaters Using Conjoint Terrestrial and Atmospheric Water Balances and Multisource Remote Sensing. *Water Resources Research*: 8608-8630. DOI:10.1029/2019WR025196

Livneh, B., Badger, A.M., Livneh, B., Badger, A.M., (2020). Drought less predictable under declining future snowpack. *Nature Climate Change*. DOI:10.1038/s41558-020-0754-8

Long, D., Bai, L., Yan, L., Zhang, C., Yang, W., Lei, H., Quan, J., Meng, X., Shi, C., (2019). Generation of spatially complete and daily continuous surface soil moisture of high spatial resolution. *Remote Sensing of Environment*: 111364. DOI:10.1016/j.rse.2019.111364

Long, D., Yan, L., Bai, L., Zhang, C., Li, X., Lei, H., Yang, H., Tian, F., Zeng, C., Meng, X., Shi, C., (2020). Generation of MODIS-like land surface temperatures under all-weather conditions based on a data fusion approach. *Remote Sensing of Environment*: 111863. DOI:10.1016/j.rse.2020.111863

Martens, B., Miralles, D., Lievens, H., Fernández-Prieto, D., Verhoest, N.E.C., Martens, B., Miralles, D., Lievens, H., Fernández-Prieto, D., Verhoest, N.E.C., (2016). Improving terrestrial evaporation estimates over continental Australia through assimilation of

SMOS soil moisture. *International Journal of Applied Earth Observation and Geoinformation*. DOI:10.1016/j.jag.2015.09.012

Martens, B., Miralles, G.D., Model, L.H., (2017). GLEAM v3: Satellite-based land evaporation and root-zone soil moisture. *GLEAM v3: Satellite-based land evaporation and root-zone soil moisture*. DOI:10.5194/gmd-10-1903-2017

Milly, P.C.D., Dunne, K.A., Milly, P.C.D., Dunne, K.A., (2020). Colorado River flow dwindles as warming-driven loss of reflective snow energizes evaporation. *Science*. DOI:10.1126/science.aay9187

Miralles, D.G., Holmes, T.R.H., Jeu, D.R.A.M., Gash, J.H., Meesters, A., Dolman, A.J., (2011). Global land-surface evaporation estimated from satellite-based observations. *Hydrology and Earth System Sciences*: 453-469. DOI:10.5194/hess-15-453-2011

Padrón, R.S., Gudmundsson, L., Decharme, B., Ducharne, A., Lawrence, D.M., Mao, J., Peano, D., Krinner, G., Kim, H., Seneviratne, S.I., (2020). Observed changes in dry-season water availability attributed to human-induced climate change. *Nature Geoscience*: 477-481. DOI:10.1038/s41561-020-0594-1

Pritchard, H.D., (2019). Asia's shrinking glaciers protect large populations from drought stress. *Nature*, 569(7758): 649-654. DOI:10.1038/s41586-019-1240-1

Qi, J., Wang, L., Zhou, J., Song, L., Li, X., Zeng, T., (2019a). Coupled Snow and Frozen Ground Physics Improves Cold Region Hydrological Simulations: An Evaluation at the upper Yangtze River Basin (Tibetan Plateau). *Journal of Geophysical Research: Atmospheres*, 124(23): 12985-13004. DOI:10.1029/2019JD031622

Qi, W., Zhang, C., Fu, G., Zhou, H., (2015). Global Land Data Assimilation System data assessment using a distributed biosphere hydrological model. *Journal of Hydrology*, 528: 652-667. DOI:10.1016/j.jhydrol.2015.07.011

Qi, W., Zhang, C., Fu, G., Sweetapple, C., Zhou, H., (2016a). Evaluation of global fine-resolution precipitation products and their uncertainty quantification in ensemble discharge simulations. *Hydrology and Earth System Sciences*, 20(2): 903-920. DOI:10.5194/hess-20-903-2016

Qi, W., Zhang, C., Fu, G., Zhou, H., (2016b). Quantifying dynamic sensitivity of optimization algorithm parameters to improve hydrological model calibration. *Journal of Hydrology*, 533: 213-223. DOI:10.1016/j.jhydrol.2015.11.052

Qi, W., Liu, J., Chen, D., (2018). Evaluations and Improvements of GLDAS2.0 and GLDAS2.1 Forcing Data's Applicability for Basin Scale Hydrological Simulations in the Tibetan Plateau. *Journal of Geophysical Research: Atmospheres*, 123(23): 13128-13148. DOI:10.1029/2018JD029116

Qi, W., Liu, J., Leung, F., (2019b). A framework to quantify impacts of elevated CO2 concentration, global warming and leaf area changes on seasonal variations of water resources on a river basin scale. *Journal of Hydrology*, 570: 508-522. DOI:10.1016/j.jhydrol.2019.01.015

Qi, W., Liu, J., Xia, J., Chen, D., (2020). Divergent sensitivity of surface water and energy variables to precipitation product uncertainty in the Tibetan Plateau. *Journal of Hydrology*, 581: 124338. DOI:10.1016/j.jhydrol.2019.124338

Rabus, B., Eineder, M., Roth, A., Bamler, R., (2003). The shuttle radar topography mission—a new class of digital elevation models acquired by spaceborne radar. *ISPRS Journal of Photogrammetry and Remote Sensing*, 57(4): 241-262. DOI:10.1016/s0924-2716(02)00124-7

Shrestha, M., Wang, L., Koike, T., Xue, Y., Hirabayashi, Y., (2010). Improving the snow physics of WEB-DHM and its point evaluation at the SnowMIP sites. *Hydrology and Earth System Sciences*, 14(12): 2577-2594. DOI:10.5194/hess-14-2577-2010

Shrestha, M., Koike, T., Hirabayashi, Y., Xue, Y., Wang, L., Rasul, G., Ahmad, B., (2015). Integrated simulation of snow and glacier melt in water and energy balance‐based, distributed hydrological modeling framework at Hunza River Basin of Pakistan Karakoram region. *Journal of Geophysical Research: Atmospheres*, 120(10): 4889-4919. DOI:10.1002/2014JD022666

Staudinger, M., Stahl, K., Seibert, J., (2014). A drought index accounting for snow. *Water Resources Research*, 50(10): 7861-7872. DOI:10.1002/2013WR015143

Tian, L., Li, H., Li, F., Li, X., Du, X., Ye, X., (2018). Identification of key influence factors and an empirical formula for spring snowmelt-runoff: A case study in mid-temperate zone of northeast China. *Scientific Reports*, 8(1): 16950. DOI:10.1038/s41598-018-35282-x

Tolson, B.A., Shoemaker, C.A., (2008). Efficient prediction uncertainty approximation in the calibration of environmental simulation models. *Water Resources Research*, 44(4): W04411. DOI:10.1029/2007wr005869

Tolson, B.A., Asadzadeh, M., Maier, H.R., Zecchin, A., (2009). Hybrid discrete dynamically dimensioned search (HD-DDS) algorithm for water distribution system design optimization. *Water Resources Research*, 45(12): W12416. DOI:10.1029/2008WR007673

Wang, L., Koike, T., Yang, D.W., Yang, K., (2009a). Improving the hydrology of the Simple Biosphere Model 2 and its evaluation within the framework of a distributed hydrological model. *Hydrological Sciences Journal*, 54(6): 989-1006. DOI:10.1623/hysj.54.6.989

Wang, L., Koike, T., Yang, K., Jackson, T.J., Bindlish, R., Yang, D., (2009b). Development of a distributed biosphere hydrological model and its evaluation with the Southern Great Plains Experiments (SGP97 and SGP99). *Journal of Geophysical Research: Atmospheres*, 114(D8). DOI:10.1029/2008jd010800

Wang, L., Koike, T., Yang, K., Yeh, P.J.-F., (2009c). Assessment of a distributed biosphere hydrological model against streamflow and MODIS land surface temperature in the upper Tone River Basin. *Journal of Hydrology*, 377(1-2): 21-34. DOI:10.1016/j.jhydrol.2009.08.005

Wang, L., Zhou, J., Qi, J., Sun, L., Yang, K., Tian, L., Lin, Y., Liu, W., Shrestha, M., Xue, Y., Koike, T., Ma, Y., Li, X., Chen, Y., Chen, D., Piao, S., Lu, H., (2017). Development of a land surface model with coupled snow and frozen soil physics. *Water Resources Research*, 53(6): 5085-5103. DOI:10.1002/2017WR020451

Xie, P., Chen, M., Yang, S., Yatagai, A., Hayasaka, T., Fukushima, Y., Liu, C., (2007). A Gauge-Based Analysis of Daily Precipitation over East Asia. *Journal of Hydrometeorology*, 8(3): 607-626. DOI:10.1175/jhm583.1

Yang, D., 1998. Distributed hydrological model using hillslope discretization based on catchment area function: development and applications, University of Tokyo, Tokyo.

Yang, X., Lin, E., Ma, S., Ju, H., Guo, L., Xiong, W., Li, Y., Xu, Y., Yang, X., Lin, E., Ma, S., Ju, H., Guo, L., Xiong, W., Li, Y., Xu, Y., (2007). Adaptation of agriculture to warming in Northeast China. *Climatic Change*. DOI:10.1007/s10584-007-9265-0

Yatagai, A., Kamiguchi, K., Arakawa, O., Hamada, A., Yasutomi, N., Kitoh, A., (2012). APHRODITE: Constructing a Long-Term Daily Gridded Precipitation Dataset for Asia Based on a Dense Network of Rain Gauges. *Bulletin of the American Meteorological Society*, 93(9): 1401-1415. DOI:10.1175/bams-d-11-00122.1

Zhang, B., Xia, Y., Huning, L.S., Wei, J., Wang, G., AghaKouchak, A., (2019). A Framework for Global Multicategory and Multiscalar Drought Characterization Accounting for Snow Processes. *Water Resources Research*. DOI:10.1029/2019WR025529

Zhang, Y., Yan, S., Lu, Y., (2010). Snow Cover Monitoring Using MODIS Data in Liaoning Province, Northeastern China. *Remote Sensing*, 2(3): 777-793. DOI:10.3390/rs2030777

Zhu, Z., Bi, J., Pan, Y., Ganguly, S., Anav, A., Xu, L., Samanta, A., Piao, S., Nemani, R.R., Myneni, R.B., (2013). Global Data Sets of Vegetation Leaf Area Index (LAI)3g and Fraction of Photosynthetically Active Radiation (FPAR)3g Derived from Global Inventory Modeling and Mapping Studies (GIMMS) Normalized Difference Vegetation

Index (NDVI3g) for the Period 1981 to 2011. *Remote Sensing*, 5(2): 927-948. DOI:10.3390/rs5020927

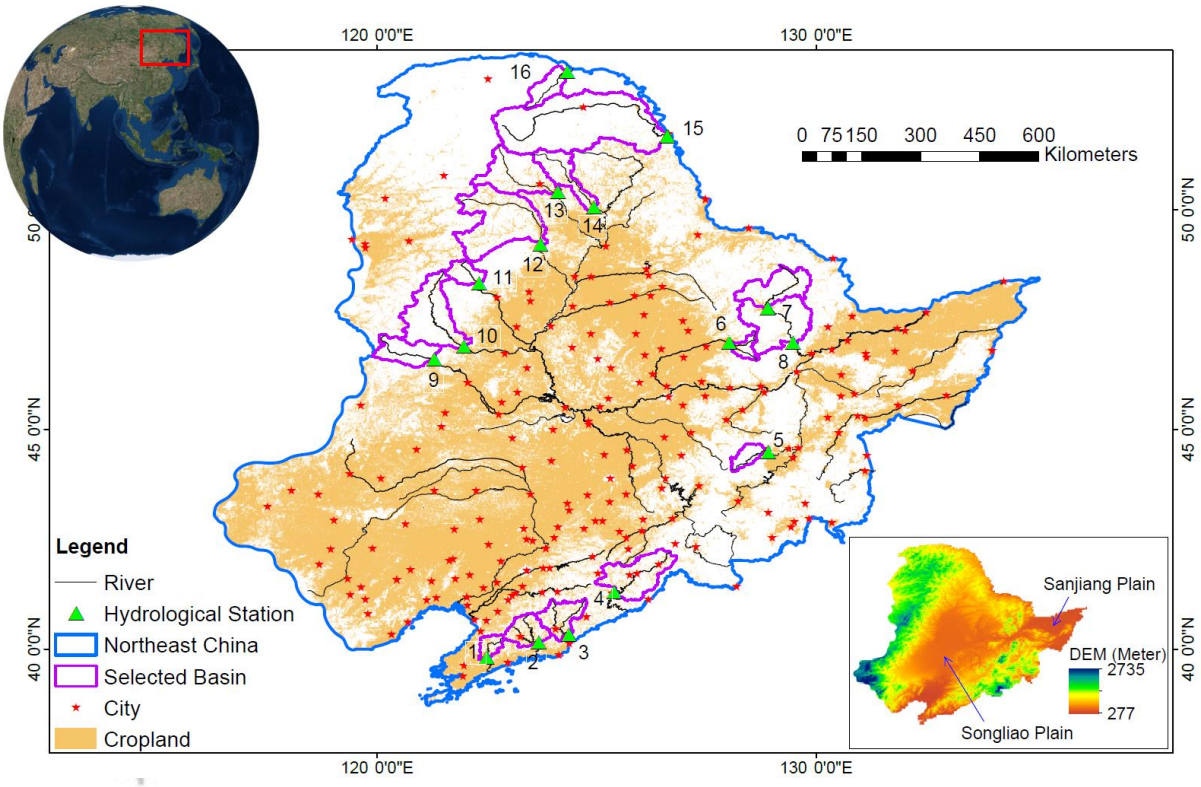

Fig. 1 The study region. The cropland distribution is from http://waterdata.iwmi.org/applications/irri_area/.

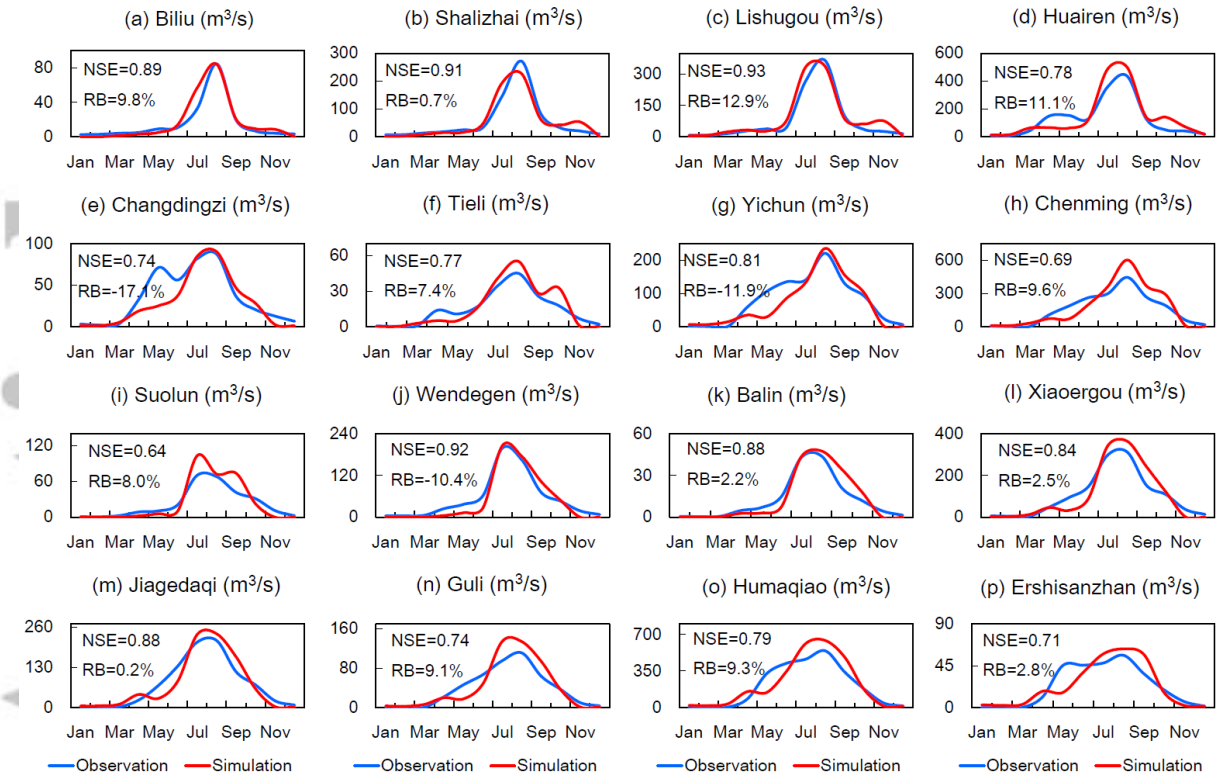

Fig. 2 Comparisons between observed and simulated discharge in the time periods studied.

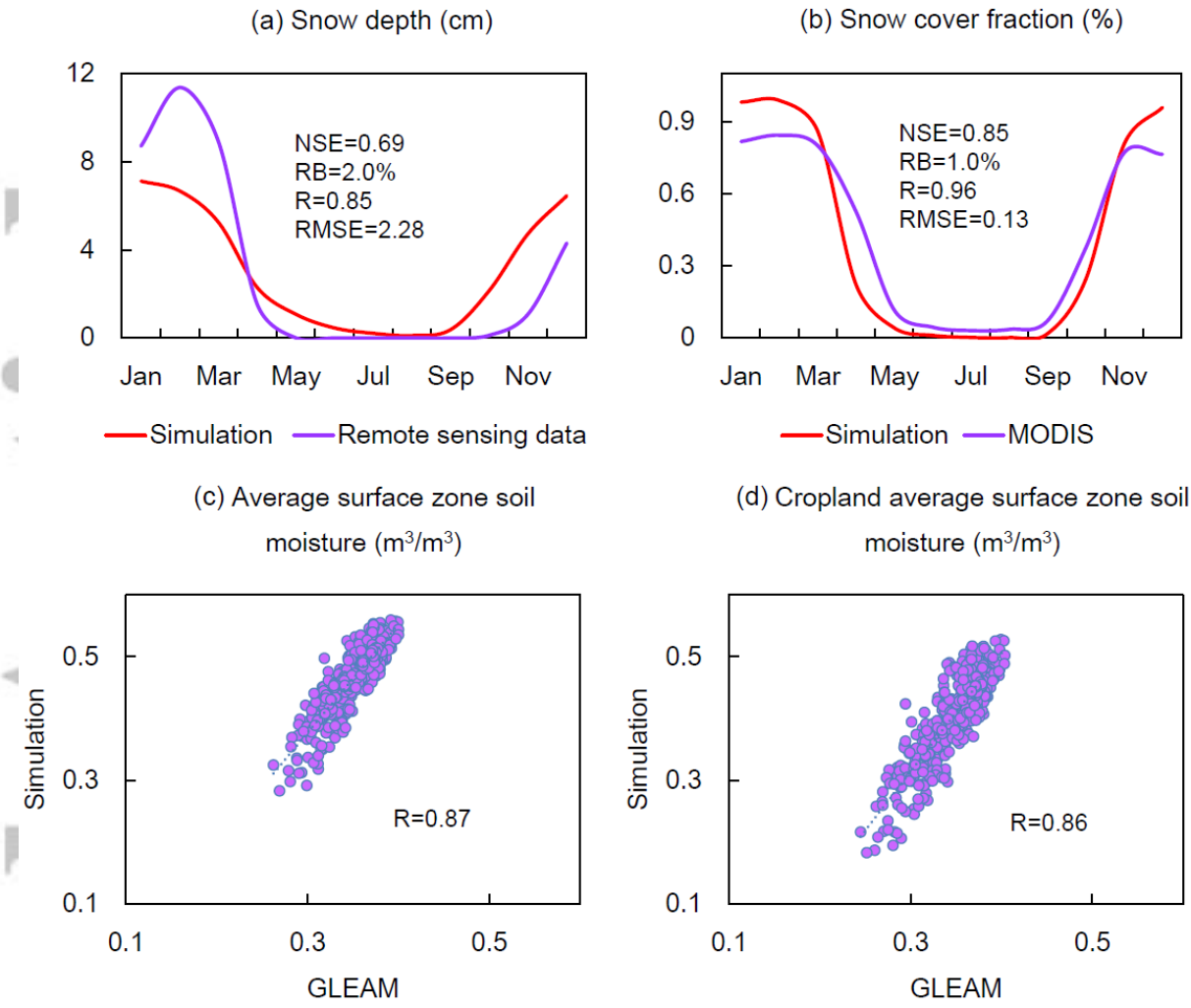

Fig. 3 (a) and (b) show average snow depth and snow cover fraction (snow covered area/total area) comparison between model simulation and remote sensing data on a multi-year mean monthly scale. (c) and (d) show comparison of surface zone soil moisture between model simulation and GLEAM datasets. (a), (c) and (d) are based on results from 1982 to 2011. Surface soil = 5 cm. MODIS = Moderate-resolution Imaging Spectro-radiometer; GLEAM = Global Land Evaporation Amsterdam Model; NSE = Nash-Sutcliffe Efficiency coefficient; RB = Relative Bias; R = Correlation Coefficient; RMSE = Root Mean Square Error.

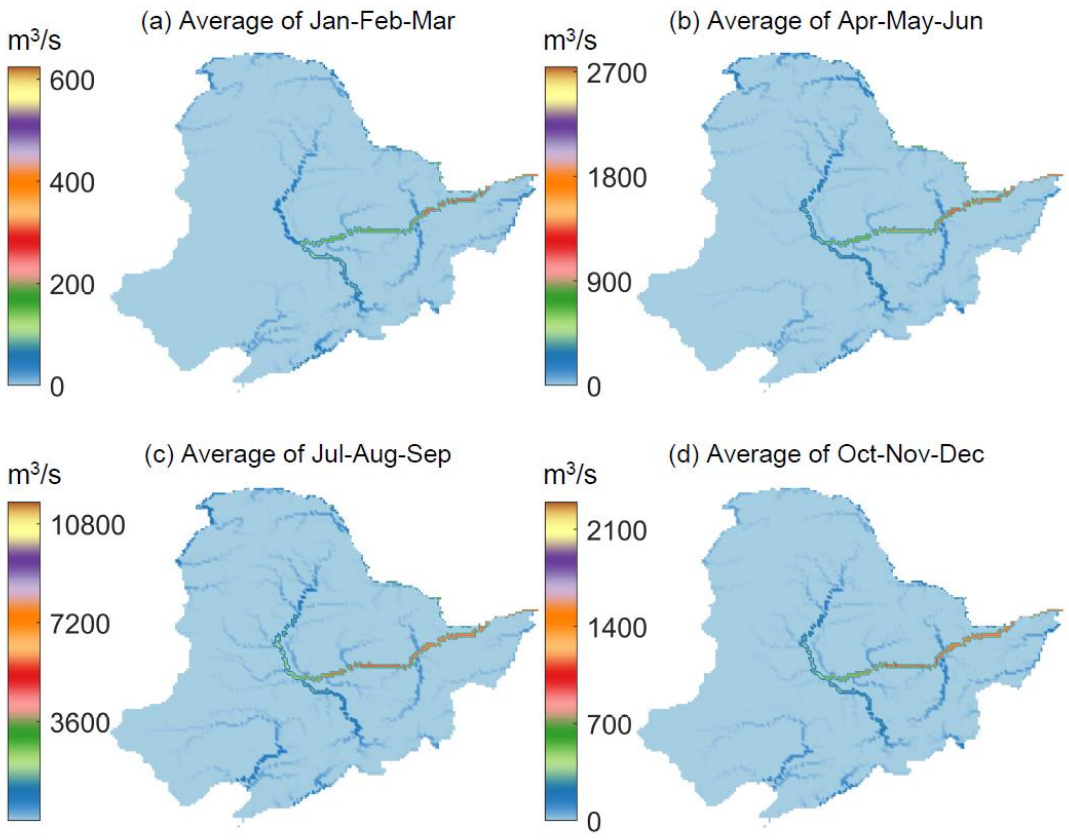

Fig. 4 Spatial distribution of simulated river discharge based on results from 1982 to 2011.

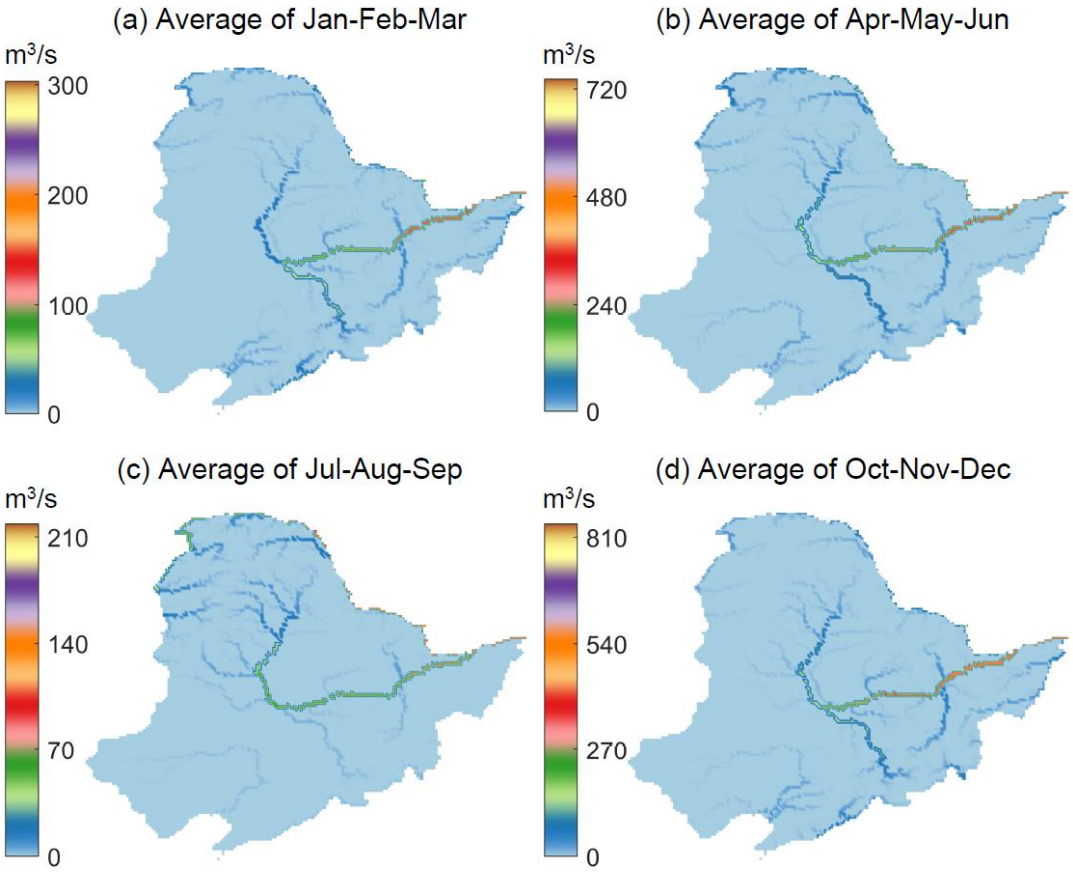

Fig. 5 Spatial distribution of simulated snow discharge based on results from 1982 to 2011.

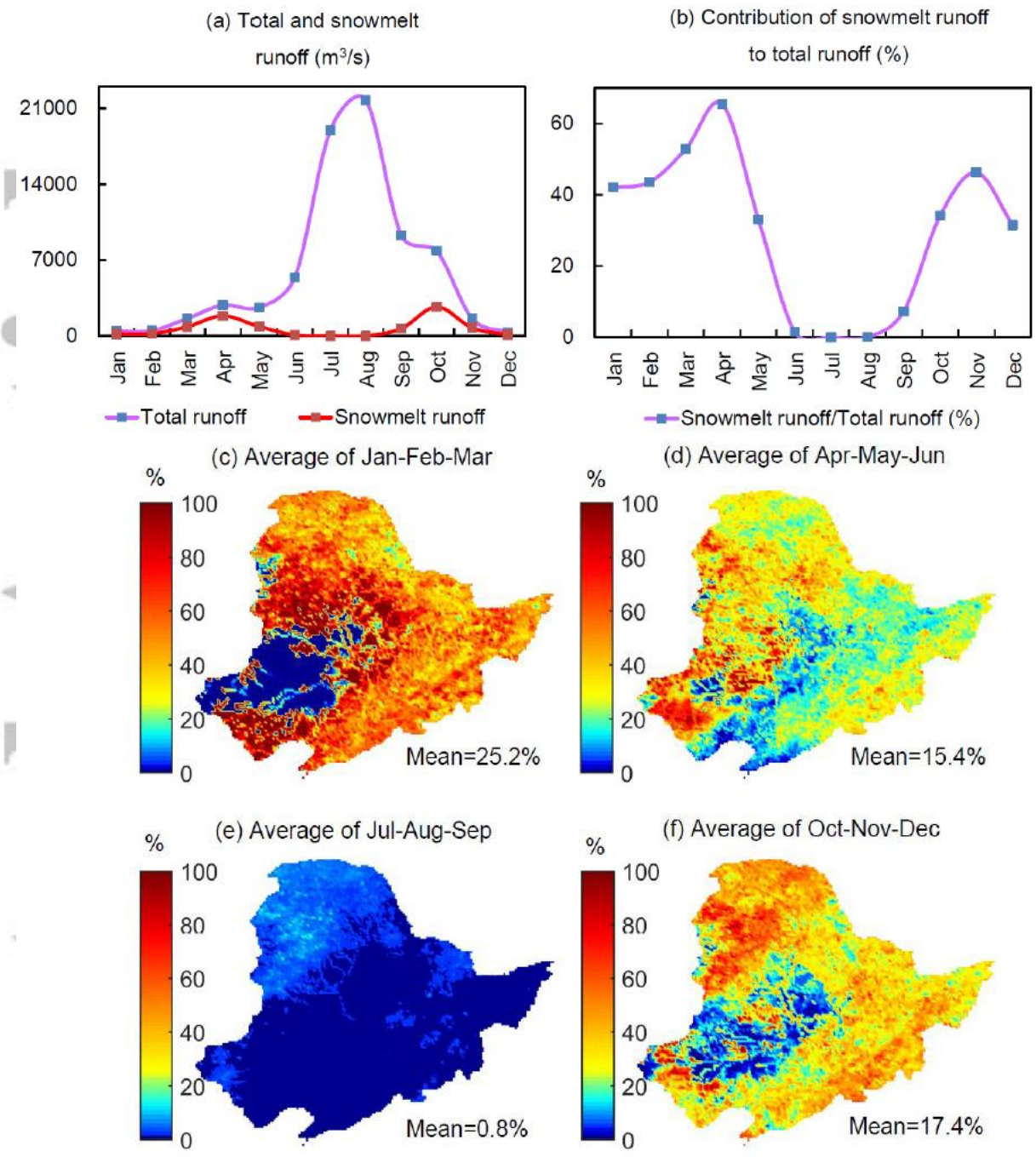

Fig. 6 Temporal changes of snowmelt runoff and contribution to total runoff (a, b), and spatial distribution of snow discharge contributions to discharge (c, d, e, f). The results are based on data from 1982 to 2011.

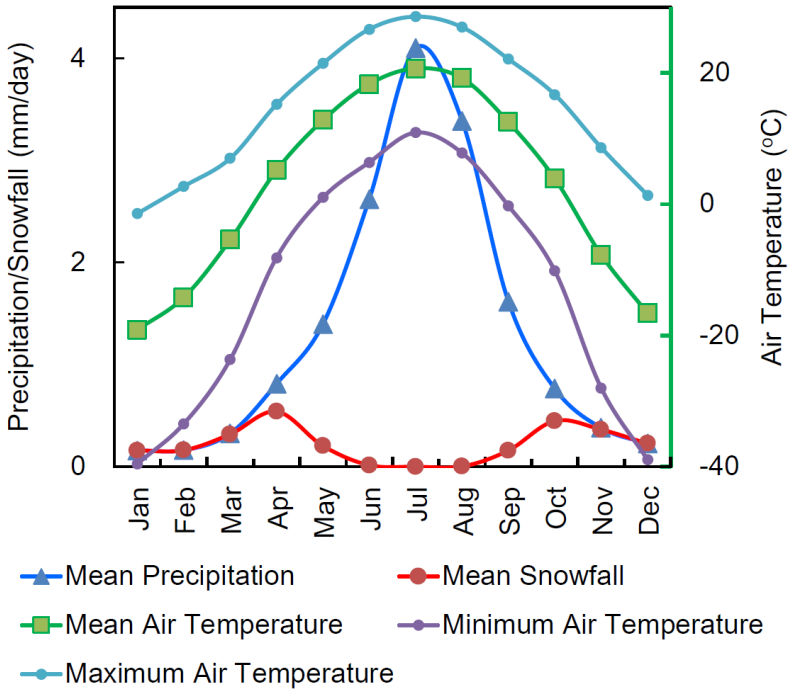

Fig. 7 Mean precipitation, mean snowfall, mean air temperature, minimum and maximum air temperature in different months in Northeast China based on data from 1982-2011.

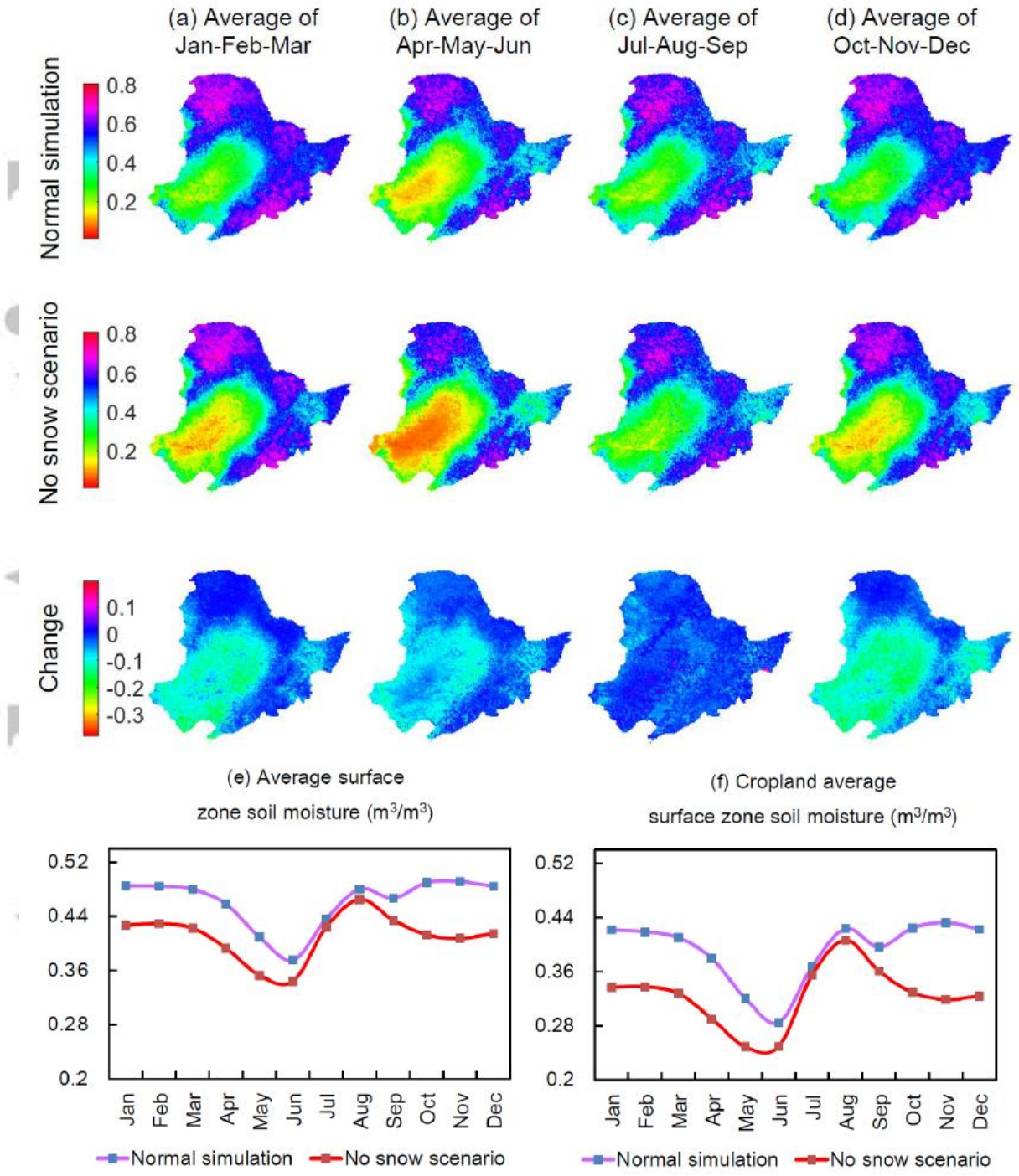

Fig. 8 Spatial distribution of surface soil moisture (a, b, c, d). In the 'No snow scenario', the snow is assumed to fall as rain. Change = soil moisture$_{\text{No snow scenario}}$ - soil moisture$_{\text{Normal simulation}}$. Change<0 means the surface soil gets dryer when no snow; Change>0 means the surface soil gets wetter when there is no snow. (e) and (f) show average surface zone soil moisture changes in Northeast China and on the cropland in the region. The results are based on data from 1982 to 2011.

Table 1 Correlation Coefficient (R) values and significance level (in the brackets) between SSdI and SSI/SRI

Accumulation time	Time lag (month)	1	2	3	4	5	6	7	8
1-month (Jan)	SSI	0.35 (0.00)	0.31 (0.00)	0.26 (0.00)	0.23 (0.00)	0.19 (0.00)	0.12 (0.02)	0.12 (0.03)	0.06 (0.25)
	SRI	0.30 (0.00)	0.29 (0.00)	0.20 (0.00)	0.14 (0.01)	0.04 (0.47)			
2-month (Jan-Feb)	SSI	0.37 (0.00)	0.32 (0.00)	0.25 (0.00)	0.21 (0.00)	0.16 (0.00)	0.10 (0.06)		
	SRI	0.39 (0.00)	0.25 (0.00)	0.20 (0.00)	0.11 (0.04)	0.03 (0.57)			
3-month (Jan-Mar)	SSI	0.35 (0.00)	0.31 (0.00)	0.25 (0.00)	0.19 (0.00)	0.14 (0.01)	0.09 (0.10)		
	SRI	0.39 (0.00)	0.30 (0.00)	0.17 (0.00)	0.11 (0.04)	0.04 (0.50)			
4-month (Jan-Apr)	SSI	0.31 (0.00)	0.28 (0.00)	0.24 (0.00)	0.19 (0.00)	0.13 (0.01)	0.08 (0.15)		
	SRI	0.37 (0.00)	0.30 (0.00)	0.21 (0.00)	0.10 (0.06)				
5-month (Jan-May)	SSI	0.28 (0.00)	0.25 (0.00)	0.20 (0.00)	0.16 (0.00)	0.11 (0.05)	0.05 (0.32)		
	SRI	0.31 (0.00)	0.27 (0.00)	0.21 (0.00)	0.13 (0.01)	0.03 (0.54)			
6-month (Jan-Jun)	SSI	0.23 (0.00)	0.21 (0.00)	0.18 (0.00)	0.14 (0.01)	0.10 (0.07)			
	SRI	0.23 (0.00)	0.21 (0.00)	0.18 (0.00)	0.12 (0.03)	0.05 (0.36)			
7-month (Jan-Jul)	SSI	0.18 (0.00)	0.18 (0.00)	0.15 (0.00)	0.12 (0.02)	0.09 (0.09)			
	SRI	0.18 (0.00)	0.16 (0.00)	0.14 (0.01)	0.12 (0.03)	0.07 (0.19)			